

Supporting Information

An innovative electrochemiluminescent immunosensor using
dual amplified signals from AuNPs@CoSn(OH)₆ for the
detection of AD-biomarker: amyloid-beta 1-40

Jiaojing Sun^{1‡}, Wenqing Geng^{2‡}, Yueju Wang², Huiling Li^{2, 3}, Rong Tan^{1,4}, and
Yifeng Tu^{1*}*

¹ College of Chemistry, Chemical Engineering and Material Science, Soochow University, Suzhou, 215123, P. R. China.

² First Affiliated Hospital of Soochow University, Suzhou, 215006, P. R. China.

³ Nursing School, Suzhou Medical College of Soochow University, Suzhou, 215006, P. R. China.

⁴ School of Material Engineering, Changshu Institute of Technology, Suzhou, 215500, P. R. China.

Section 1 The chemicals and instruments

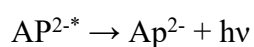
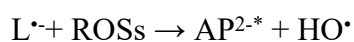
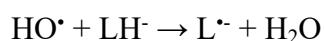
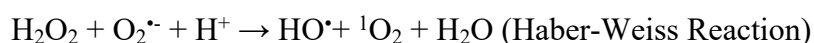
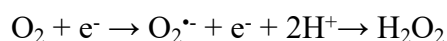
All chemicals used in this study are of analytical grade, and ultrapure water with a resistance of 18.25 M Ω ·cm is employed throughout the experiments. NaH₂PO₄ Na₂HPO₄ were purchased from Sinopharm Chemical Reagent Co. Ltd. (Shanghai, China). SnCl₄·5H₂O and Co(NO₃)₂·6H₂O were purchased from Shanghai Macklin Biochemical Technology Co. Ltd. (Shanghai, China). Trisodium citrate dihydrate (Na₃C₆H₅O₇·2H₂O) and 3-aminopropyltrimethoxysilane (APTMS) were supplied by Shanghai Aladdin Biochemical Technology Co. Ltd. (Shanghai, China). NaOH was purchased from Shanghai Lingfeng Chemical Reagent Co. Ltd. (Shanghai, China). Chloroauric acid (HAuCl₄·3H₂O, 99.9%) and PDDA (M_w=400000-500000, 20 wt % in water) were purchased from Shanghai Titan Scientific Co. Ltd. (Shanghai, China). Luminol was obtained from Fluka Chem. Co. Ltd. (Beijing, China). Recombinant human amyloid beta peptide 1-40 was purchased from Shanghai Kanglang Biological Technology Co. Ltd. (Shanghai, China). Amyloid beta 1-40 antibody and A β ₄₀ ELISA kit were obtained from Shanghai Huzhen Industrial Co. Ltd. (Shanghai, China). Indium tin oxide-coated glass (ITO) was supplied by Guluo Glass Electronics Co. Ltd. (Luoyang, China). Plasma samples were provided by the cooperating laboratory at the First Affiliated Hospital of Soochow University.

All of the ECL experiments were carried out on a lab-built apparatus (see details in Section 2). The use of sensor will be included in a three-electrode system together with an Ag/AgCl reference electrode and a Pt wire auxiliary electrode. A SU8010 scanning electron microscope (Hitachi, Japan) and a HT7700 transmission electron microscope (Hitachi, Japan) were utilized to observe the morphology, size and distribution of nanomaterials. X-ray diffraction (Bruker, Germany) analysis was applied to reflect the crystal face and crystallinity of nanomaterials and X ray photoelectron spectroscopy (Thermo Scientific, America) was used to investigate elemental composition and valence status. An Agilent UV-vis absorption spectrometer, a Zeta Potential Analyzer (Malvern, UK) are utilized in experiments. An RST-5200 electrochemical workstation (Suzhou Risetest Instruments Co. Ltd., China) was set up to carry out cyclic voltammetry (CV) and electrochemical impedance spectroscopy (EIS) tests.

Section 2 The installation and principle of ECL testing instrument.

It provides a pulsed voltage with independently adjustable upper/lower limiting potentials and periods for the electrolysis of luminol, along with an optical detection system based on photomultiplier tube powered by a negative high voltage. Here a computer-based digital pulse generator (DPG) serves as the source of pulse waveform, which then controls the potentiostat via an analog-to-digital converter to drive the three-electrode system which comprises platinum wire as the auxiliary electrode, an Ag/AgCl reference electrode, and a biosensor as the working electrode. The ECL signal is generated on sensor surface when apposite potential is applied to the electrode system. Then, the ECL signal will be converted to a current by the photomultiplier tube (PMT) as the optical detector, which is driven by a high negative voltage. Finally, an amplification/conversion circuit (including A/D converter) will then be activated to record the signal in a computer. In the ECL testing, a pulsed electrolytic voltage is used to trigger the redox of the luminescent probe and co-reactant.

To obtain the highest luminous efficiency, duty ratio, period and upper/lower limiting potentials must be optimized. Lower limiting potential (usually negative) induces the reduction of dissolved oxygen to yield ROSs, while higher limiting potential (usually positive) causes the oxidization of luminol to the intermediate free radical. Energy transfer from ROSs to luminol free radicals on the electrode surface intensifies ECL emission because of the generation of numerous additional excitons. The yielding of ROSs is a relatively complex process. Under the lower limiting potential of pulsed electrolytic voltage, the reduction of dissolved O₂ converts to many ROSs including O₂^{•-}, H₂O₂, OH[•], ¹O₂ etc., via a cascade Haber–Weiss reaction. The primary steps of ROSs production and the enhancement mechanism of luminol ECL may be reflected in the equations below:



Section 3 The characterization and performance optimization of AuNPs@CoSn(OH)₆ nanocomposite.

By controlling the mole fraction of sodium citrate added in solution A, CoSn(OH)₆ with different sizes can be prepared. A smaller amount of sodium citrate results in larger size of the nanomaterial. CoSn(OH)₆ nanoparticles of different sizes (100-150 nm, 200-300 nm, and 400-500 nm) were prepared by adding 1 mmole, 0.8 mmole, and 0.6 mmole sodium citrate, respectively. As shown in Fig. S1 A-C, the SEM images present morphologies of nanocubes of different sizes.

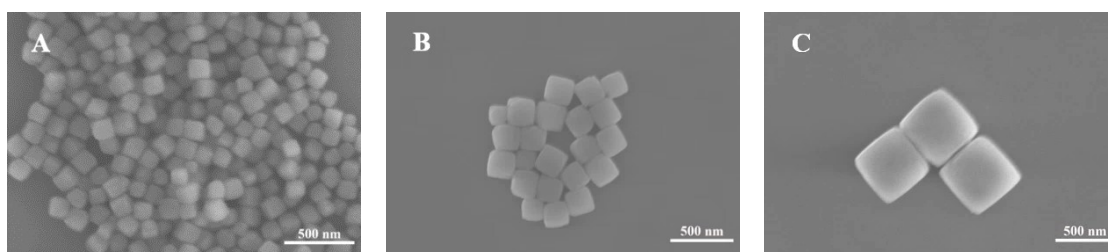


Fig. S1 The SEM images of CoSn(OH)₆ of different sizes: (A) 100-150 nm, (B) 200-300 nm, (C) 400-500 nm.

The size variation of nanomaterial will affect the strengthen of the ECL signal of luminol, with the most effective catalytic performance at a size of 100-150 nm (Fig. S2). It also shows the most even distribution on ITO electrodes, as shown in Fig. S3.

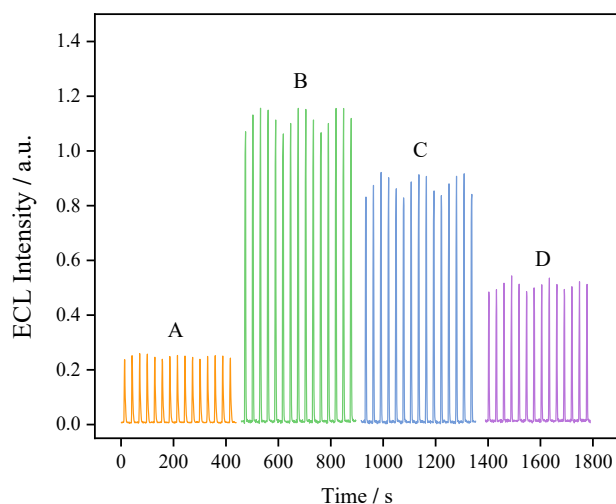


Fig. S2 ECL intensity of luminol on (A) blank ITO or functioned ITO electrodes with (B) 100-150 nm, (C) 200-300 nm, (D) 400-500 nm CoSn(OH)₆.

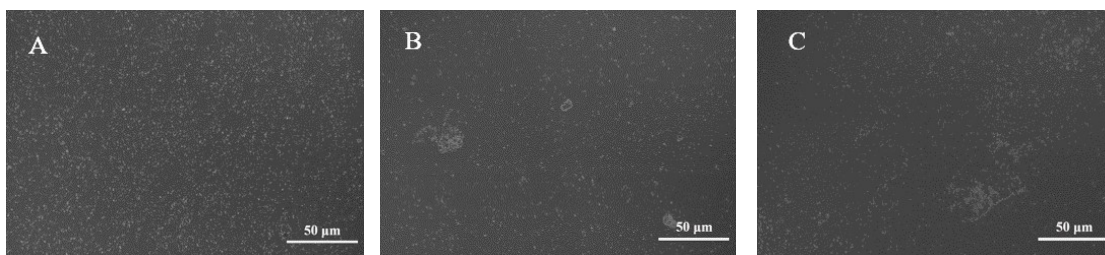


Fig. S3 The distributions of CoSn(OH)_6 on ITO: (A) 100-150 nm, (B) 200-300 nm, (C) 400-500 nm.

It is impossible to attach AuNPs to CoSn(OH)_6 without external assistance because both are negatively charged. Poly(dimethyldiallylammonium chloride) (PDDA) is a cationic polyelectrolyte that can effectively solve this problem. The usage of PDDA needs to be optimized considering its low conductivity; both too little and too much PDDA will not be beneficial for optimal performance. Fig. S4 reveals that the ECL signal of luminol will reach its highest when 1 mL of PDDA is used.

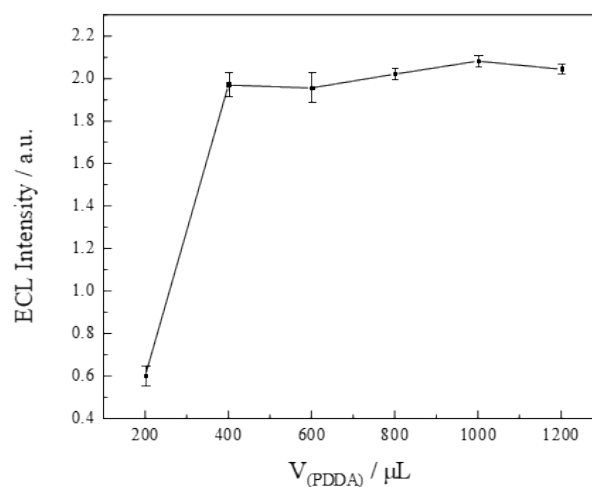


Fig. S4 The optimization of the usage of PDDA for optimal performance.

The size of AuNPs has a great impact on the overall performance of nanocomposite and the amplifying effect on the ECL of luminol¹. As shown in Fig. S5 A-D, AuNPs with diameters ranging from 10 to 35 nm were successfully prepared and loaded onto CoSn(OH)_6 . Fig. S5 E and F show that the nanomaterial made with 11 mL of gold nanoparticles with a diameter of 15 nm has the best performance.

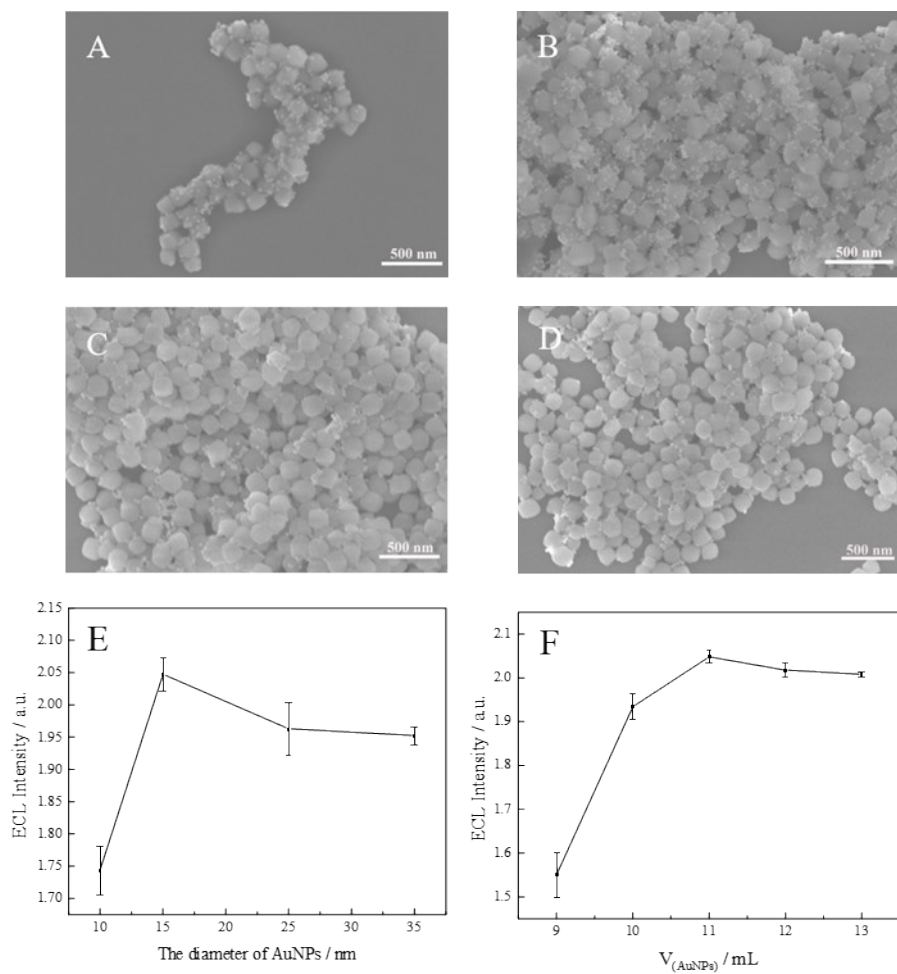


Fig. S5 The SEM images of nanomaterials made with AuNPs of diameters (A) 10 nm, (B) 15 nm, (C) 25 nm and (D) 35 nm. The optimization of (E) the diameter of AuNPs and (F) the usage of AuNPs for maximum ECL enhancement.

Section 4 The characterization of AuNPs@CoSn(OH)₆ nanocomposite

As shown in Figure S6A, the survey scan XPS spectrum indicates the presence of Co, Sn, O, and Au elements in AuNPs@CoSn(OH)₆, corresponding to the results of EDS. In Figure S6B, two primary peaks are located at 797.6 and 781.3 eV, corresponding to Co 2p_{1/2} and Co 2p_{3/2}². According to reports, cobalt (III) oxide can be differentiated from cobalt (II) oxide due to the lack of multi-electron excitation satellites³. Thus, the clear satellite peaks manifest that the Co element keeps the status of +2 in CoSn(OH)₆. For the Sn 3d spectrum (Fig. S6C), the two typical peaks (3d_{5/2} and 3d_{3/2}) are located at 486.7 eV and 495.2 eV with a peak splitting of 8.5 eV, indicating that Sn is in the +4 oxidation state. The XPS spectrum of O 1s can be divided into two peaks at 532.6 and 531.4 eV (Fig. S6D), corresponding to the oxygen in physically adsorbed water molecules and the lattice oxygen of hydroxide structure, respectively. The XPS spectrum of Au 4f (Fig. S6E) shows two main peaks at 87.4eV and 83.7eV, which are assigned to Au 4f_{5/2} and Au 4f_{7/2}, respectively. These results fully demonstrate the successful preparation of the nanocomposite.

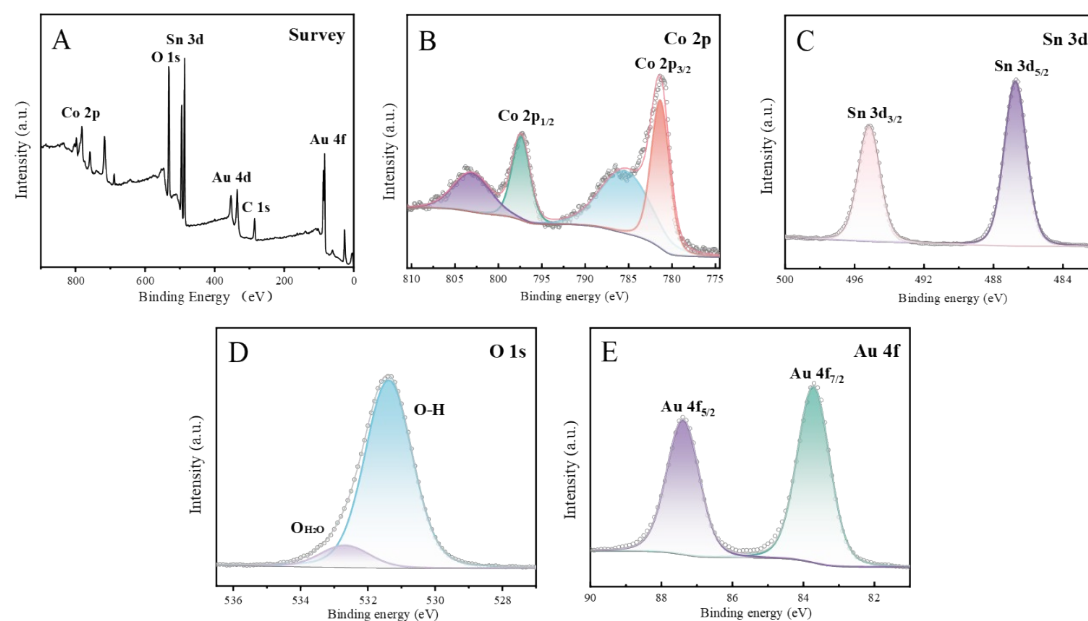


Fig. S6 (A) XPS survey spectrum of AuNPs@CoSn(OH)₆. XPS spectra of the elements (B) Co 2p, (C) Sn 3d, (D) O 1s and (E) Au 4f

Section 5 The optimization of sensing performance

In order to obtain the maximum sensing signal, all the parameters involved in the fabrication process also need to be optimized. The concentration of APTMS used to functionalize the electrode has a significant effect, as shown in Fig. S7A. Too low concentration will not be able to link up enough nanocomposite, while too high concentration will severely impede electron transfer to inhibit the ECL signal. It is observed that the optimal concentration of APTMS for loading AuNPs@CoSn(OH)₆ is 0.01%. Fig. S7B and C depict that the optimal content of nanocomposite is 0.18 mg/mL and the optimal deposition time is 2h.

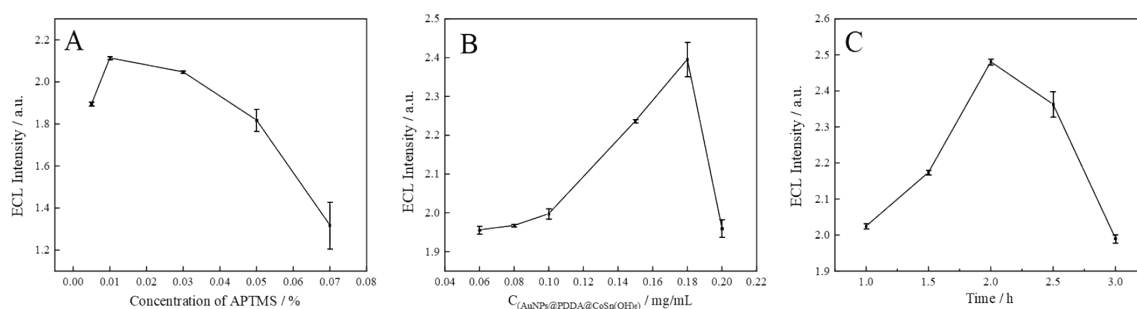


Fig. S7 The optimization of (A) the concentration of APTMS, (B) the content of AuNPs@CoSn(OH)₆ nanocomposite, and (C) the deposition time of nanocomposite on ITO electrode.

In ECL testing, a continuous pulse voltage is applied to the electrode, in which the upper and lower limiting potentials are the key factors in luminol ECL reaction. The former promotes the oxidation of luminol to produce free radicals, and the latter affects the conversion rate of dissolved O₂ into ROSs. As shown in Fig. S8(A-C), the ECL intensity reaches the highest when the upper limiting potential is 1.3 V, the lower limiting potential is -0.4 V, and the pulse period is 3 s.

Furthermore, the pH of the buffer solution also affects the ECL emission of luminol. When the pH of PBS buffer is 8.0 (Fig. S8D), the amplification multiple of the signal reaches the maximum.

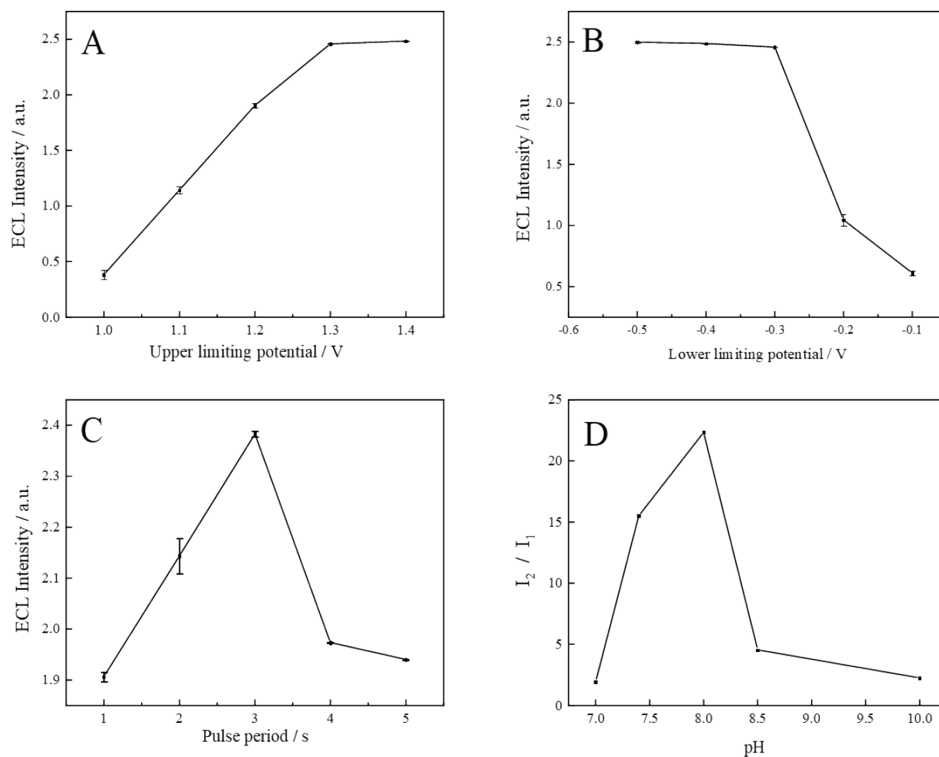


Fig. S8 The optimization of ECL conditions on AuNPs@CoSn(OH)₆/ITO: (A) upper limiting potential, (B) lower limiting potential, (C) pulse period and (D) the pH of the PBS buffer solution.

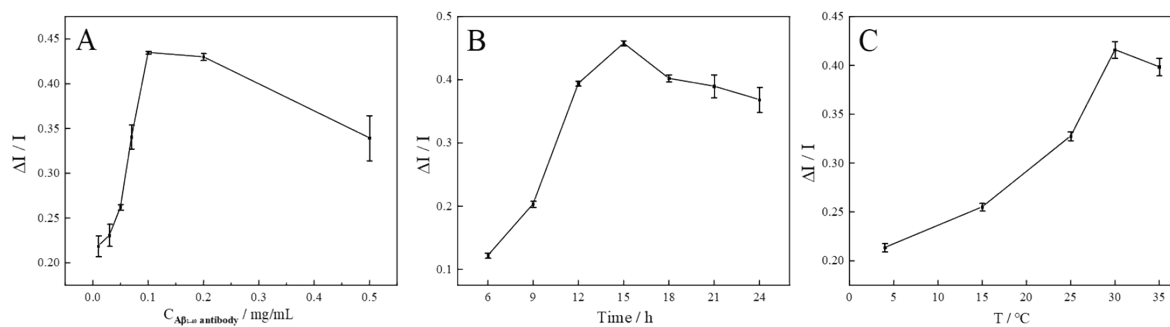


Fig. S9 Optimization of the conditions for immunosensor fabrication: (A) the concentration of the antibody A β_{40} ; (B) the temperature and (C) the time for antibody incubation.

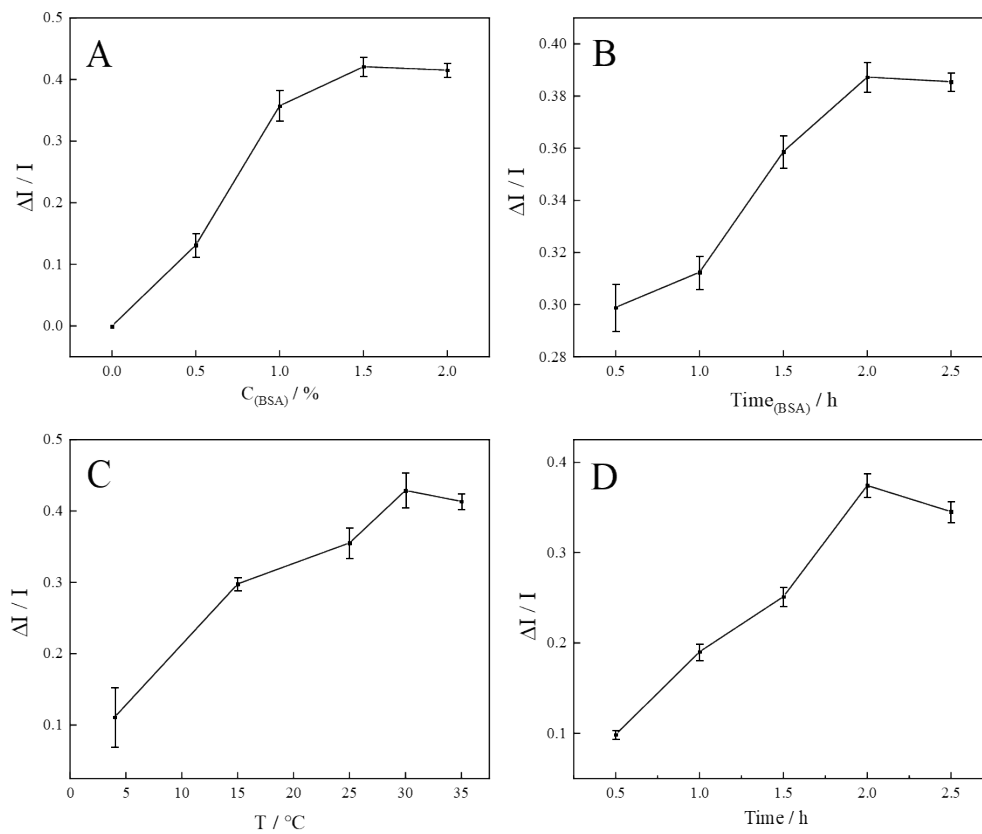


Fig. S10 Optimization of the conditions for immunosensor fabrication: (A) the concentration of BSA; (B) the time for BSA incubation. The optimization of the conditions for $A\beta_{40}$ detection: (C) the temperature and (D) the time for $A\beta_{40}$ incubation on the immunosensor.

Section 6 The performance of developed ECL immunosensors for detecting A β ₄₀ compared with other methods

Table S1. Analytical performance comparison of various methods for A β ₄₀ detection.

Method	Linear range (pg/mL)	LOD (pg/mL)	References
Differential pulse voltammetry	$(2-40) \times 10^6$	4×10^6	4
H ₂ O ₂ production (TMB)	$4 \times 10^2 - 2 \times 10^5$	128.4	5
EIS ([Fe(CN) ₆] ^{3-/4-})	$40 - 4 \times 10^5$	40	6
p-AP redox (TCEP)	$2 \times (10^3 - 10^5)$	22.5	7
LSV-Met (35) redox	9-2250	6.63	8
ECL	1-800	0.47	This work

References

1. Y. Higashi, J. Mazumder, H. Yoshikawa, M. Saito and E. Tamiya, *Analytical Chemistry*, 2018, **90**, 5773-5780.
2. R. Sahoo, A. K. Sasmal, C. Ray, S. Dutta, A. Pal and T. Pal, *ACS Applied Materials & Interfaces*, 2016, **8**, 17987-17998.
3. J. Yang, H. Liu, W. N. Martens and R. L. Frost, *The Journal of Physical Chemistry C*, 2010, **114**, 111-119.
4. M. Chikae, T. Fukuda, K. Kerman, K. Idegami, Y. Miura and E. Tamiya, *Bioelectrochemistry*, 2008, **74**, 118-123.
5. Y. Yu, X. Sun, D. Tang, C. Li, L. Zhang, D. Nie, X. Yin and G. Shi, *Biosensors and Bioelectronics*, 2015, **68**, 115-121.
6. A. Kaushik, P. Shah, P. K. Vabbina, R. D. Jayant, S. Tiwari, A. Vashist, A. Yndart and M. Nair, *Analytical Methods*, 2016, **8**, 6115-6120.
7. L. Liu, Q. He, F. Zhao, N. Xia, H. Liu, S. Li, R. Liu and H. Zhang, *Biosensors and Bioelectronics*, 2014, **51**, 208-212.
8. T. C. Liu, Y. C. Lee, C.-Y. Ko, R.-S. Liu, C.-C. Ke, Y.-C. Lo, P.-S. Hong, C.-Y. Chu, C.-W. Chang, P.-W. Wu, Y.-Y. Chen and S.-Y. Chen, *Theranostics*, 2018, **8**, 4210-4225.